CHARACTERISATION OF DISLOCATION BEHAVIOUR IN RPV STEEL

G. Monnet, C. Domain
EDF, France;
D. Bacon
University of Liverpool;
D. Terentyev
SCK CEN

Results obtained in the framework of the European project PERFECT (FI60-CT-2003-208840) are presented.

1. MD SIMULATIONS OF SLIP ON {112} PLANES

1.1. Atomic model of the edge dislocation

The simulation model developed by Osetsky and Bacon [1] was employed to study the edge dislocation in the (011) base plane and also modified to create the edge dislocation in the (112) plane. Both dislocations are created with a Burgers vector $\boldsymbol{b} = ½[11\bar{1}]$. In the case of the (112) dislocation, the principal axes x, y and z of the simulated BCC crystal were oriented along the $[11\bar{1}]$, $[\bar{1}10]$ and $[112]$ directions, respectively.

The straight edge dislocation with slip plane x-y was created along the y direction and had Burgers vector $\boldsymbol{b} = ½[11\bar{1}]$ parallel to the x axis. Periodic boundary conditions were applied along the x and y directions. The box was divided into three parts along z. The upper and lower parts consisted of several atomic planes in which atoms were rigidly fixed in their original positions (block F) or displaced following the applied loading conditions (block D). Atoms in the inner region were free to move (block M). A glide force on the dislocation was generated by the displacement of the block D in the x direction (AD) or in the –x direction (TD), which corresponds to simple shear strain γ. The corresponding resolved shear stress induced by the applied deformation was calculated as $\tau = F_x/A_{xy}$, where F_x is the total force projected in the x direction and computed from all atoms in block D and A_{xy} is the xy cross-section area of the box.

Static simulations were performed in order to compute the structure, the elastic energy and the Peierls barrier of the edge dislocation. The relaxation of the atomic motion has been performed using a combination of conjugate gradient algorithm followed by quasidynamic relaxation (quenching). The strain increment was 10^{-6} which provides sufficient accuracy of the estimation of the stress [1]. The size of the crystallite used for static simulations was $140\sqrt{3}/2\times60\sqrt{2}\times24\sqrt{6}$ (lattice units), the amount of freely mobile atoms was ~1.3 M.

MD simulations were performed to obtained stress-strain curves corresponding to the shear deformation under constant strain rate applied in two opposite [111] directions at different temperatures (from 10 up to 200 K). The size of the crystallite used for MD simulations was the same as for static simulations along y and z axes and $50\sqrt{3}/2$ along x direction and the amount of freely mobile atoms was ~450000.

The interatomic potential for bcc Fe developed by Ackland et al. [2] was used. The integration of Newton's equations was performed using a constant time step equal to 5 and 1 fs for simulations at low (1-50 K) and high (above 50 K) temperatures, respectively.

1.2. Dislocation core structure and the Peierls model

Inspired from the dislocation Peierls model [3], a convenient way to represent the core structure of the edge dislocation (ED) is to build the distribution of displacements in the atomic planes on both sides of the slip plane. However, in the case of the (112) dislocation, the BCC lattice implies to remove or add three (111) half planes on one side of the slip plane in order to create the edge dislocation.

The periodicity in the $[11\bar{1}]$ is different from that in the [112] direction. In addition, the $(11\bar{1})$ is not a mirror plane. This suggests

that the (112) dislocation has an asymmetrical core structure. The Generalised Stacking Fault Energy (GSFE) is responsible for the decrease of the dislocation core size. It can be obtained from ab-initio (first-principles) calculation. The comparison between the case of the $(\bar{1}10)$ and the (112) SFE can be found in Fig. 1.

The comparison shows that when the GSFE is asymmetrical, the dislocation core structure is also asymmetrical.

Consequently, the connection between the different physical features of the dislocation core structure, i.e. the displacements in the upper and lower layers, the local equilibrium condition and the GSFE cannot be established through the PN model.

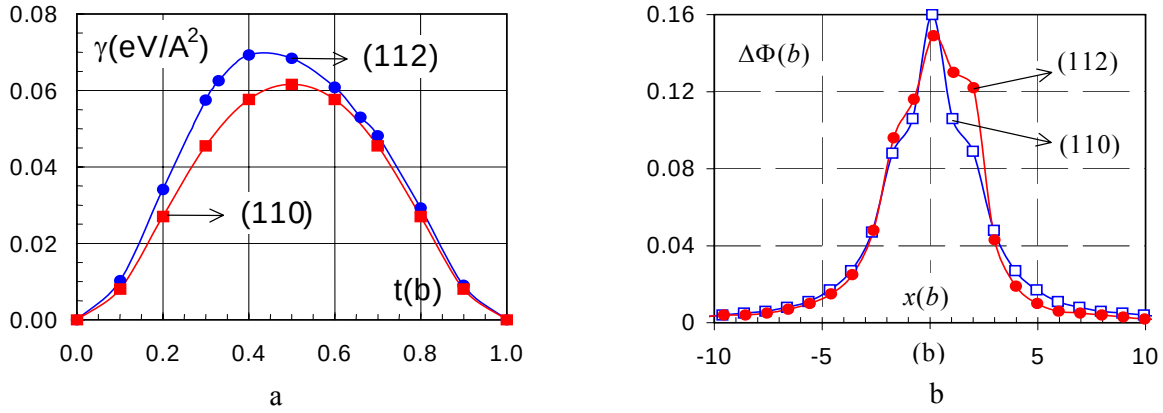

Fig.1. Effect of the asymmetry of GSFE of the core structure: energy of staking fault in the $(\bar{1}10)$ and (112) planes (a) and the differential disregistery in the $(\bar{1}10)$ and (112) dislocation core structures (b)

1.3. Effect of temperature on the stress-strain curves

MD simulations of plastic shear in the TD and AD senses were performed at different temperatures at fixed strain rate (10^7 s^{-1}), using the same MD box ($50\sqrt{3}/2\times60\sqrt{6}\times24\sqrt{2}$) and adjusting the equilibrium lattice unit and MD time step. It is important to note here that, given the large dislocation density in the MD simulation box, the dislocation velocity amounts only to some m/s, which is quite usual in mechanical tests. The large strain rate does not lead, in our simulations, to large dislocation velocities observed in shock wave propagation. Stress-strain curves extracted from the simulations are presented in Fig. 2 for the two directions of load. The critical stress needed for the dislocation motion decreases drastically with temperature; it reaches half Peierls stress already at 10 K. At T=200 K, the maximum stress measured over the whole simulation period did not exceed 15 MPa for both directions of load, as shown in Fig. 2.

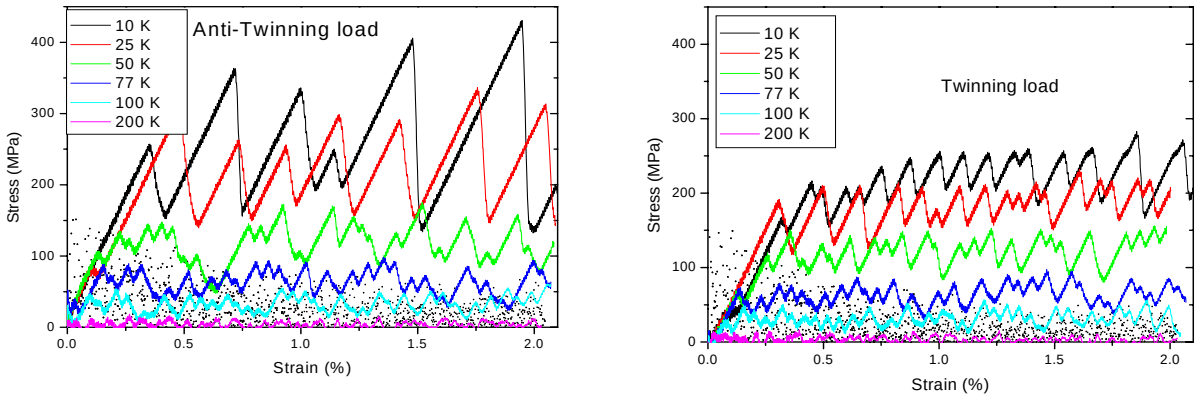

Fig. 2. Loading curves of the (112) dislocation in the twinning and antitwinning directions as a function of temperature

At low T (10 & 25 K), however, there is a remarkable difference in the stress-strain curves obtained for TD and AD loads. In particular, applying AD deformation, the

critical stress is clearly higher and the frequency of drops is lower, than in the case of TD load. The larger drop in the stress suggest that the length of a dislocation jump, while moving from Peierls valley to another one, is different in these two cases.

Using visualisation tools we have looked at the motion of the dislocation core in detail. The location of the dislocation core and identification of atoms belonging to it was realised as described above. Following the motion of the dislocation core is has been revealed that dislocation may move via different mechanisms depending on temperature. At T=0 K, the {112} edge dislocation experiences a rigid motion of its entire length over the Peierls valley.

In the absence of thermal activation, the rigid motion in the both loading directions requires a large quantity of mechanical work. The stress level is of the same order of magnitude, as that needed for the motion of the ½<111> screw dislocation [6].

At finite temperature, the dislocation is found to move with the help of the nucleation and propagation of double-kinks alone its line. Every stress drop corresponds to a jump over several Peierls valley. In other terms, although the stress is decreasing during the drop, double-kinks continue to nucleate on the dislocation line.

On the other hand, since the motion of the (112) edge dislocation is controlled at low temperature by the nucleation of the double-kinks, one expects the mobility to follow the same law as that of screw dislocation, i.e. proportionality to the dislocation length weighted the Boltzmann factor. One can thus apply the same treatment proposed by Domain et al. [6] in which the following equation was proposed to deduce the value of critical stress from the stress-strain curve:

$$\tau_c = \frac{kT}{V} \ln \left\langle \exp \frac{V\tau}{kT} \right\rangle ,$$

where V is the activation volume, k the Boltzmann constant. Here we note that the value of the τ_c is slightly dependent on the activation volume. An approximate value of V is therefore enough to obtain an approximate value of the critical stress. In order to have a rough approximation of V, we performed MD simulation at T = 77 K and used different strain rates [4]. Assuming the maximum stress as proportional to the critical stress, the activation volume was estimated close to $4b^3$. Assuming that this value of V slightly varies at different temperature, the critical stress as a function temperature can be evaluated.

1.4. Conclusion

The Peierls stress for the motion of the (112) dislocation in both senses is very large compared to that of the (110) dislocation. This suggests that the <111>(112) slip systems is little active at low temperature. But this strong Peierls resistance is shown to decrease strongly with temperature thanks to thermal activation. Edge dislocations can therefore move in both senses at almost the same stress as those in the (110) slip planes.

2. DATABASE OF INTERACTION FORCES FOR EDGE DISLOCATIONS AND RADIATION DEFECTS USING DIFFERENT POTENTIALS

The aim of this research is to compare the results of earlier computer simulations of the interaction between edge dislocations and defect clusters created by radiation damage in α-iron (Fe) with similar studies using a more recent interatomic potential. Two types of cluster have been treated, namely self-interstitial atom (SIA) loops and voids.

The earlier research used the interatomic potential for α-Fe developed in 1997 by Ackland et al. [2], but recent simulation studies indicate that the potential derived by Ackland, Mendelev and co-workers in 2004 [5] provides a more realistic model for point defects, their clusters and screw dislocations [6-8]. Thus, it was planned that some of the previous work on the interaction of edge dislocations with intrinsic defects such as voids and SIA loops would be repeated with the new potential in order to check the validity of the atomic mechanisms and values of critical stress, τ_c, found earlier. This was considered necessary because some defect clusters have been shown to provide sufficiently high obstacle strength that the branches of the dislocation at the cluster are pulled into a screw-dipole configuration at τ_c, and it is the behaviour of the screw that

distinguishes the two potentials. We have examined the core structure of the infinitely long, straight, ½<111>{1 $\bar{1}$ 0} edge dislocation in the two models. There is no significant difference. However, the critical resolved shear stress for dislocation glide at T = 0 K (the Peierls stress) for the two models is distinctly different, i.e. about 83 MPa with the 2004 potential compared with just under 25 MPa with the older one. Furthermore, the steady-state dislocation velocity under the same applied resolved shear stress and temperature is significantly lower with the 2004 potential, as shown in Fig. 3. We have not found an explanation for these differences in dislocation behaviour in the two models.

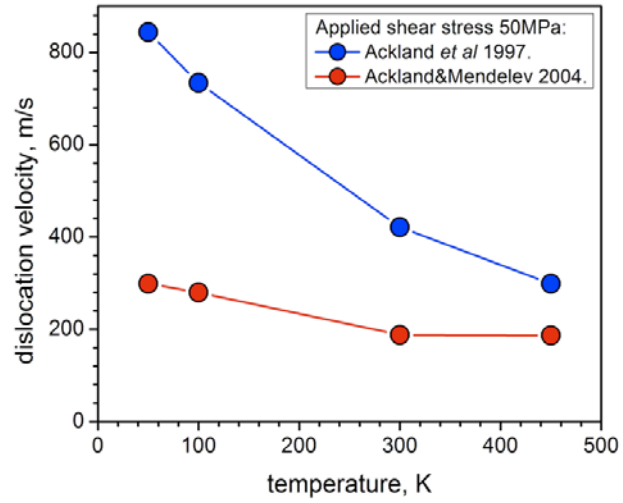

Fig. 3. Velocity vs temperature for edge dislocations in models of Fe under constant applied resolved shear stress of 50 MPa

2.1. Dislocation-SIA loop interaction

The atomic-scale dynamics of an edge dislocation interacting with self-interstitial atom (SIA) loops was described in the report for month 24 [9]. The effects analysed and modelled involve either (a) loop drag by a gliding dislocation when the loop Burgers vector ***b*** is parallel to the glide plane, or (b) intersection when ***b*** is inclined to the glide plane, resulting in either absorption for small loops or dislocation pinning before breakaway for large loops. Papers on this research have been published [10].

The simulations treated an edge dislocation with ***b*** = ½[111] interacting with SIA loops with ***b*** = ½[1 $\bar{1}$ 1], which is inclined to the dislocation glide plane (1 $\bar{1}$ 0), and containing either 37 or 331 interstitials. Such a loop is attracted to the dislocation in both cases. Small loops are easily absorbed as jogs on the dislocation at all T by rotation of their Burgers vector to ½[111] and are relatively weak obstacles to dislocation glide, whereas large loops react to form segments with ***b*** = [010] and are strong obstacles. The mechanisms observed are broadly consistent with those for the large loops, but τ_c at low T (i.e. 0 or 1 K) is high (~530 MPa). The results are published in [11].

We have now carried out simulations of loops with 169 SIAs using the 1997 potential in order to compare results for loops of the same size. The τ_c values obtained to date are summarised in Fig. 4,a. It is seen that although the critical stress at low T is much higher (by a factor of two) with the 2004 potential, there is little difference in the critical stress between the two models at 300 K. The data in Fig. 4,a also show that the applied strain rate ('sr') has little effect on τ_c.

On the basis of these results, we conclude that differences between dislocation-loop interactions are probably not significant for temperature conditions of interest ($T \geq$300 K), but to confirm this completely we are now determining τ_c at 600 K with the 1997 potential. Fig. 4,b contains the data of Fig. 4,a together with τ_c for 37-SIA and 331-SIA loops. It is clear that there is a marked transition in obstacle strength between loops with 37 SIAs and those with 169. Furthermore, the effect of loop size is small for loops that form <010> segments on reacting with the gliding dislocation.

Finally, we are also simulating loops with ***b*** = <100> using the two potential models and will present the results in the next report.

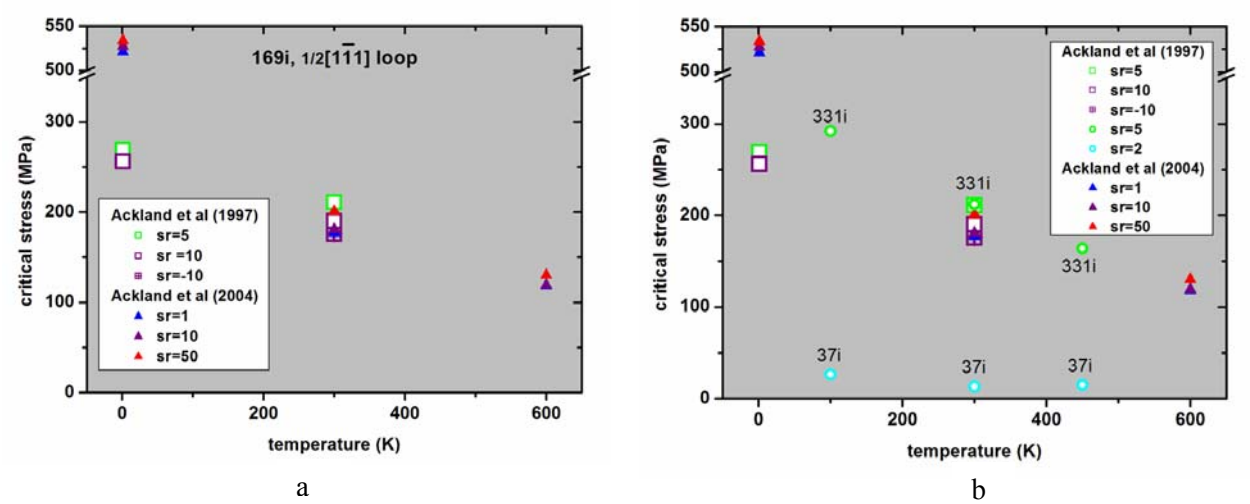

Fig. 4. Comparison of τ_c for an edge dislocation with b = ½<111> breaking away from a row of interstitial loops with b = ½[1-11] for the 1997 and 2004 interatomic potentials. Applied strain rate is in units of 10^6 s^{-1}. Loops containing 169 SIAs (a); As (a) plus data from [10] for loops containing either 37 or 331 SIAs (b)

2.2. Dislocation-void interaction

This difference in behaviour seen above for loops at low temperature ($T \sim 0$ K) is also apparent in the interaction between an edge dislocation and a periodic row of voids. Fig. 5 shows dislocation line shape at the maximum (critical) stress, τ_c, for the two potentials. The void diameter is 2 nm. It is seen that the line on one side of the void in the model based on the 2004 potential (Fig. 5,b) is strongly aligned with the $[11\bar{1}]$ direction at 70° to ***b***, which is horizontal in these figures. Estimates of the elastic line tension indicate that this alignment effect is not due to elastic anisotropy: it is assumed to arise from trapping of the dislocation core in this orientation. On the other hand, although no voids do not form at 0 K, it is important theoretically to investigate the response of the material at 0 K with pre-existing obstacles as voids. In fact, at finite temperature, thermal activation can only decrease the obstacle strength. The response obtained at 0 K represents therefore the maximum strength of the defect.

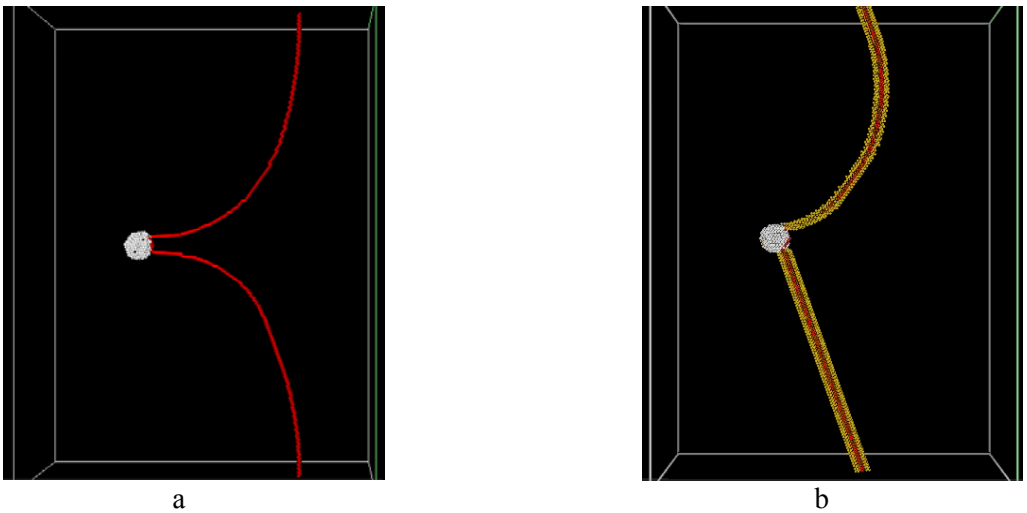

Fig. 5. Dislocation line shape in the glide plane at the critical stress for a periodic row of voids (diameter = 2 nm and centre-to-centre spacing 41.4 nm) in α-Fe at T = 0 K. The Burgers vector direction is horizontal in these visualizations. The 1997 interatomic potential (a); the 2004 potential (b)

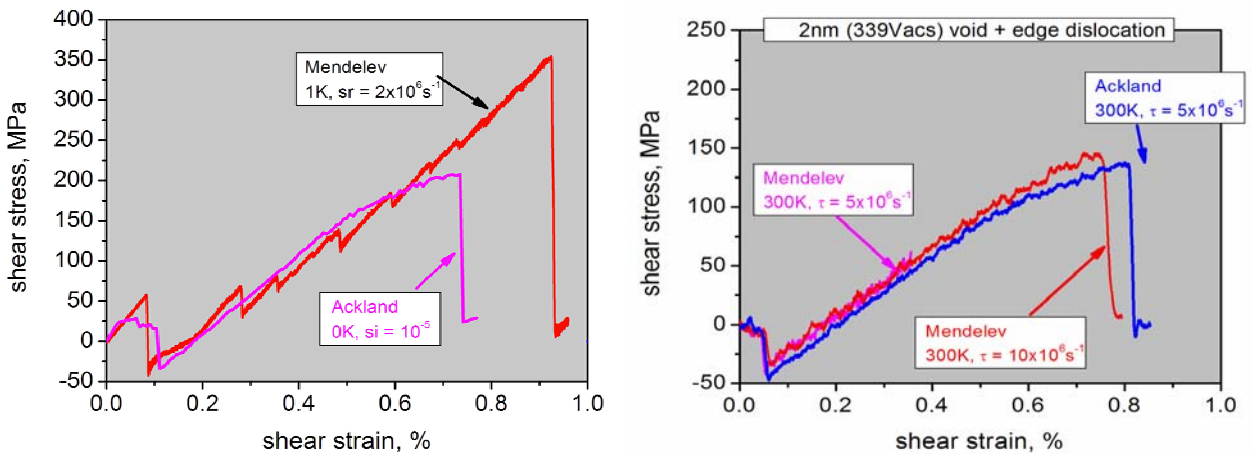

a b

Fig. 6. Comparison of the stress vs. strain plots for an edge dislocation cutting and breaking away from the periodic row of voids in Fig. 1 at (a) low T and (b) 300 K. 'Ackland' and 'Mendelev' refer to the 1997 and 2004 interatomic potentials [2,12], respectively

It results in τ_c = 350 MPa compared with just over 200 MPa found with the older potential - see the stress-strain plots in Fig. 6,a. However, the marked difference in critical stress and line shape disappears as T is raised, as illustrated by the stress-strain plots for 300 K in Fig. 6,b. This indicates that the results for void strengthening obtained previously using the 1997 potential would be consistent with those from similar simulations based on the 2004 potential. We are now testing this conclusion by analysing results of new simulations across a range of conditions of void size, temperature and strain rate.

3. DD SIMULATIONS OF CARBIDE STRENGTHENING AT LOW TEMPERATURE

3.1. Introduction

The present work is dedicated to the investigation by Dislocation Dynamics (DD) simulation of the low temperature behaviour of RPV steel.

The low temperature mechanical behaviour of RPV steel is controlled by the thermally activated motion of screw dislocations. Concerning precipitation strengthening, most of models and theoretical approaches are based on the assumption of isotropic mobility of dislocations independently of their character. Even the well established model (called in the following the BKS model) proposed by Bacon et al. [13] does not allow to predict precipitation strengthening in dynamical conditions, i.e. when the motion of dislocation is time dependent.

We use DD simulations to predict strengthening due to carbides in RPV steel. The mobility law already constructed for dislocations is found to provide a good description of dislocation behaviour at low temperature. They are therefore used to investigate the effect of carbide on the flow stress.

In the following, we present the study of the interaction of infinite dislocations with infinite periodic row of carbides. The study characterises the temperature and rate effects on the interaction. Then we show the influence of the carbide distribution on the flow stress.

3.2. Mobility laws of dislocations

In DD simulations, the mobility law that allows to deduce the velocity of a screw segment v_{vis} as function of the effective stress τ^* was fitted on experimental results using the Kocks formulas [14]. The result of fitting provides the following equation:

$$v_{vis} = H\, L \exp\left(-\frac{\Delta H_0}{kT}\right) 2 \sinh\left(\frac{\Delta H_0}{kT}\sqrt{\frac{\tau^*}{\tau_0}}\right),$$

where H and τ_o are constant, L the screw segment length and ΔH_0 the total activation energy close to 0.84 eV. The value of is 363 MPa is not considered to be representative to the Peierls stress at 0 temperature.

Concerning edge dislocations, we do not have at our disposal any experimental information about thier mobility at low

temperature. Characterisation using Molecular Dynamics (MD) simulation was only performed in pure iron and the corresponding viscous drag coefficient is not appropriate in our case of RPV steel. Therefore we make the assumption that the mobility of edge dislocation is proportional to that of screw dislocations with a factor K much larger than unity. Explicitly, the velocity of edge segment is given by:

$$v_{edge} = v_0 K \exp\left(-\frac{\Delta H_0}{kT}\right) 2\sinh\left(\frac{\Delta H_0}{kT}\sqrt{\frac{\tau^*}{\tau_0}}\right),$$

where v_0 is constant and taken equal to 10^5 µm/s. The factor K is a strongly decreasing function of temperature. This ensures that the difference in mobility between screw and non-screw segments decreases with temperature, which is in agreement with experience.

3.3. Infinite dislocation interacting with periodic row of carbides

In order to bypass difficulties related to the carbide distribution, we start first by characterising using DD simulation interactions with periodic rows of carbides. Depending of the initial character of the infinite dislocation, the nature and the force of interaction is strongly modified as we will see in the following.

3.3.1. Case of edge dislocation

Although the mobility is dependent on temperature, the length of the segment is not affecting the velocity. Also the other characters are treated in the same way as edge character. We expect the precipitation hardening to be slightly dependent on temperature.

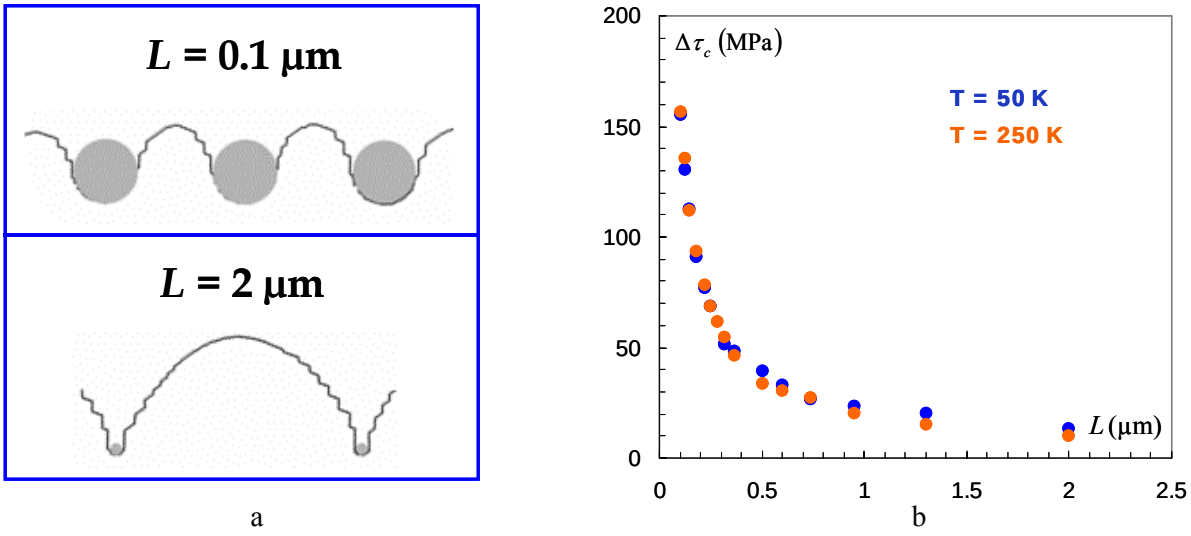

Fig. 7. Critical shape of the edge dislocation at 50 K with different carbide spacing (a) and the Orowan strengthening as a function of carbide spacing for 50 and 250 K (b)

In Fig. 7 we can see that the critical shape of the dislocation is similar to that achieved with isotropic dislocation mobility, independently of the carbide spacing. Fig. 1,b shows that the associated strengthening is almost independent of temperature and close to that predicted by the BSK model [1].

The case of non-screw dislocations is then easy to predict and similar to the interaction in the athermal regime. This is du to the fact that the screw dipole generated during the bypassing process is of low mobility in comparison with non-screw dislocations. The stress increment is therefore needed to generate the screw dipole and elongation of the latter does not involve large increase in the stress. When the screw dipole is long enough the mobility of screw dislocation increases sufficiently to enable bypassing of carbides.

3.3.2. Case of screw dislocation

Unlike edge segment, the mobility of screw segments is strongly dependent on stress and temperature and is affected by the length of the segment. DD results prove that by decreasing temperature the strengthening decreases also. It appears that strengthening follows two regimes: (i) at large precipitate spacing, the strengthening is small and

slightly dependent of the spacing and (ii) at small spacing, the strengthening decreases strongly with spacing, as shown in Fig. 2. When the temperature rises, the strengthening approaches that given in the BSK model [13] but remains below it.

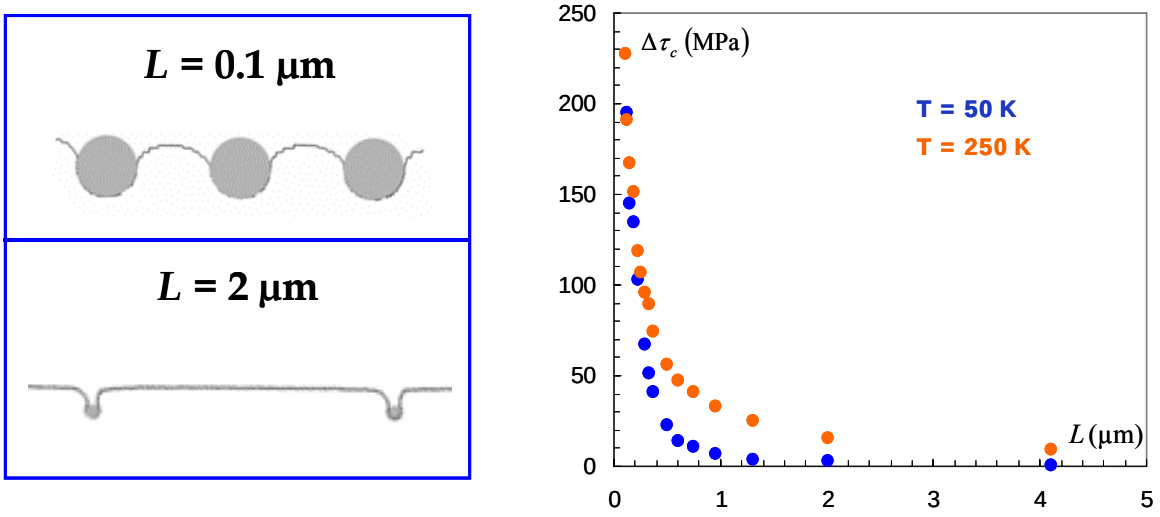

a b

Fig. 8. Critical shape of the screw dislocation at 50 K with different carbide spacing(a) and the Orowan strengthening as a function of carbide spacing for 50 and 250 K (b)

The figure shows that the mechanism is dependent on the spacing of carbide. At large spacing the dislocation is not curved while at small spacing, it adopts a critical shape close to that observed in the athermal regime. The surprising feature is that the observed strengthening is always less than theory.

3.3.3. Case of random character

An infinite dislocation of random character behaves as mixture of a screw and edge dislocation. However, the corresponding interaction is rather complicated and not introduced here for the sake of brevity. The random behaviour is investigated in the following study of the interaction with random distribution of carbides.

3.4. Carbide-induced strengthening in RPV steel

Carbides are introduced in the simulation space following the same procedure used to characterise the carbide strengthening in the athermal regime (Fig. 8). For more information about the characterisation of the carbide population, readers are invited to consult the latter report.

Here we recall only that dislocations mobility is highly anisotropic which alters the behaviour of the dislocation microstructure.

The effect of temperature on the evolution of the microstructure is depicted in Fig. 9. The difference in dislocation shape suggest large differences in the mechanical response of the system.

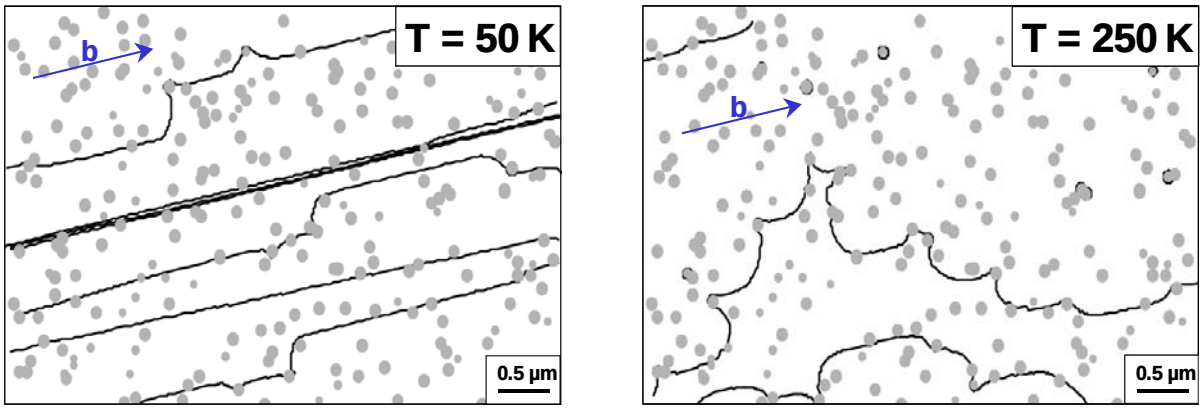

Fig. 9. Comparison between the dislocation microstructure obtained at 50 and 250 K

Here we can state some remarks from a qualitative point of view. On the one hand, at high temperature the anisotropy in dislocation mobility is small and the dislocation-line shape looks like that obtained in the athermal regime. The corresponding strengthening is therefore expected to be the same at room temperature. One the other hand, since screw dislocation at low temperature are almost not curved, we suspect the microstructure not to be affected by the carbide presence.

In order to have a more precise prediction of carbide effect on the mechanical response, 4 similar DD simulations were carried out at different temperatures, as seen in Fig. 10. The athermal strengthening is added for comparison.

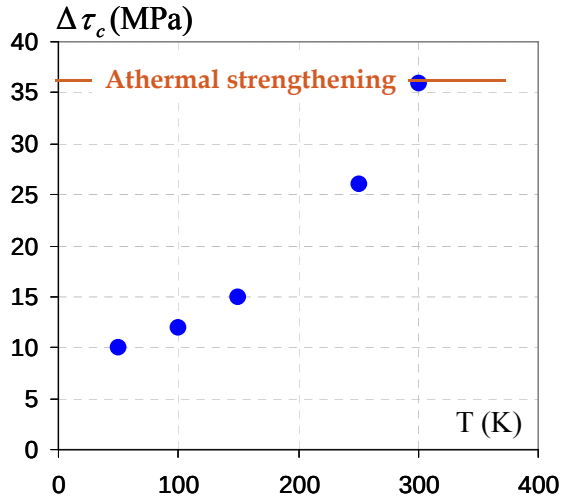

Fig. 10. Carbide induced strengthening in RPV in the athermal regime

We can see that carbide strengthening decreases strongly at low temperature. It tends to a threshold of almost 10 MPa at very low temperature. The origin of this threshold is still unknown by the author.

3.5. Conclusions

This deliverable reports DD simulation results on carbide strengthening in RPV steel at low temperature. We have shown that the interaction between dislocations and carbides depends on the local dislocation character. For screw dislocation, the strengthening is strongly dependent on the temperature, rate and carbide spacing. The strengthening is a complex function of these parameter but, in all cases, it increases with temperature. However, no significant temperature effect was observed in the case of non-screw dislocations.

The behaviour of the dislocation microstructure in the presence of random distribution of carbides is rather complex. The strengthening depends on temperature strain rate. Whatever the simulation conditions, the strengthening increases with temperature and decreases with strain rate.

REFERENCES

1. Yu.N. Osetsky and D.J. Bacon // *Model. Simul. Mater. Sci. Eng.* 2003, v. 11, p. 427.
2. G.J. Ackland, D.J. Bacon, A.F. Calder, T. Harry // *Phil Mag*. A.1997, v. 75, p. 713.
3. R.E. Peierls // *Proc. Phys. Soc*. 1940, v. 52, p. 23.
4. G. Monnet, D. Terentyev // *Acta Mater.* 2009, v.57, p.1416.
5. G.J. Ackland, M.I. Mendelev, D.J. Srolovitz, S. Han and A.V. Barashev // *J. Phys.: Condens. Matter.* 2004, v. 16, p. 2629.
6. C. Domain and G. Monnet // *Phys. Rev. Lett.* 2005, v. 95, p. 215506.
7. F. Willaime, C-C. Fu, M.C. Marinica, J. Dalla Torre // *Nucl. Instrum. & Meth. B.* 2005, v. 228, p. 92.
8. J. Chaussidon, M. Fivel and D. Rodney // *Acta Mater.* 2006, v. 54, p. 3407.
9. D.J. Bacon. Month 24 Report for PERFECT WP IV.
10. Z. Rong, Yu.N. Osetsky, and D.J. Bacon // *Phil. Mag.* 2005, v. 85, p. 1473.
11. D. Terentyev, L. Malerbal, D.J. Bacon, and Yu.N. Osetsky // *J. Phys.: Condens. Matter.* 2007, v. 19, p. 456211.
12. M.I. Mendelev, S.W. Han, D.J. Srolovitz, G.J. Ackland, D.Y. Sun, and M. Asta // *Phil. Mag*. 2003, v. 83, p. 3977.
13. D.J. Bacon, U.F. Kocks, R.O. Scattergood // *Phil. Mag.* 1973, v. 28, p. 1241.
14. U.F. Kocks, A.S. Argon, and M.F. Ashby. Thermodynamics and kinetics of slip // *Prog. Mater. Sci.* 1975, v. 19, p. 1.

ХАРАКТЕРИСТИКА ПОВЕДЕНИЯ ДИСЛОКАЦИЙ В СТАЛИ ДПЛА

Дж. Монет, С. Домейн, Д. Бейкон, Д. Терентьев

Приводятся результаты, полученные в рамках Европейского проекта PERFECT (F160-CT-2003-208840).

ХАРАКТЕРИСТИКА ПОВЕДІНКИ ДИСЛОКАЦІЙ В СТАЛІ ДПЛА

Дж. Монет, С. Домейн, Д. Бейкон, Д. Терентьєв

Наводяться результати, отримані у рамках Європейського проекту PERFECT (F160-CT-2003-208840).